Electrodynamics of Magnetic Pulse Welding Machines: Global and Local Electrical Analogues

R. Bouzerar[1,4], F. Bougrioua[1], I. Tekaya[1,4*], N. Foy[1], M. Hamzaoui[2], V. Bourny[2,3], O. Durand-Drouhin[4], D. Jouaffre[5], D. Haye[5]

[1] Laboratoire Physique des Systèmes Complexes, EA 4663, Université de Picardie Jules Verne, Amiens, France
[2] Laboratoire des Technologies Innovantes, EA 3899, Université de Picardie Jules Verne, Amiens, France
[3] ESIEE, 14 Quai de la Somme, Amiens, France
[4] Laboratoire de Physique de la Matière Condensée, EA 2081, Université de Picardie Jules Verne, France
[5] PFT Innovaltech, Lycée Condorcet, Rond-Point Joliot-Curie, Saint-Quentin, France
[*]Corresponding author. E-mail: issyan.tekaya@u-picardie.fr

Abstract

In this paper, a theoretical, experimental and numerical study of MPW machines is carried out. While it is known that such machines are very complex by nature because of the coupling between different parts, we used simple electrical analogues to describe its dynamics. A RLC circuit modeling the whole machine is depicted and experimental results are shown. A further study including numerical simulations allows to compute the current distribution and estimate the magnetic field within the coil but also the magnetic pressure generated in the process, all using a 2D model and reasonable assumptions. A late theoretical study opens the way for innovative experimental measurements regarding the kinetics of the deformations of metallic tubes, but also their mechanical behavior before the welding process, making use of their capacitive properties.

Keywords

Magnetic pulse welding, Electrodynamics, Electrical analogues

1 Introduction

Magnetic pulse technologies and especially their application to welding or forming (Broeckhove, 2010, Daehn, 2002, Psyk et al., 2011), are an important application of electromagnetism attracting the attention of both the academic and industrial communities. Because of their complexity, these technologies and related research give an interesting example of cross-disciplinary theme since it can be regarded as an application of electromagnetism and high deformation mechanics leading to potential biological risk. There is no need to stress the extreme importance of electromagnetism (Griffith, 1999) in our modern societies, so deeply permeated with its applications as telephony or radio broadcasting. But the significant development of electromagnetic technology has deeply modified the radiation bath exerted on individuals, leading to unavoidable questioning about its harmfulness. This ambient bath is particularly intense around electromagnetic sources such as the magnetic pulses machines we focus on in our study. The evaluation of the impact of electromagnetic radiation on both users' health (biological effects of radiations) and material environment (electronic devices being sensitive to electromagnetic pulses) is the first type of fundamental questions raised by the study of electromagnetic machines. These investigations can certainly profit by a better knowledge of the machine dynamics and its malfunction. More precisely, this second fundamental questioning regards the operation of such machines in connection to their structure. As any industrial machine, magnetic pulse machines convert electrical power into work (mechanical deformations of pieces), this process being accompanied with multiple sources of loss. Magnetic forming or welding machines, as schematized on **Fig. 1**, consist mainly of a power generator, that is a set of high voltages capacitances, providing, through a spark-gap (power switch), the extremely high current intensities necessary to produce the high magnetic pulses or equivalently the magnetic stresses required to deform hard conductive materials.

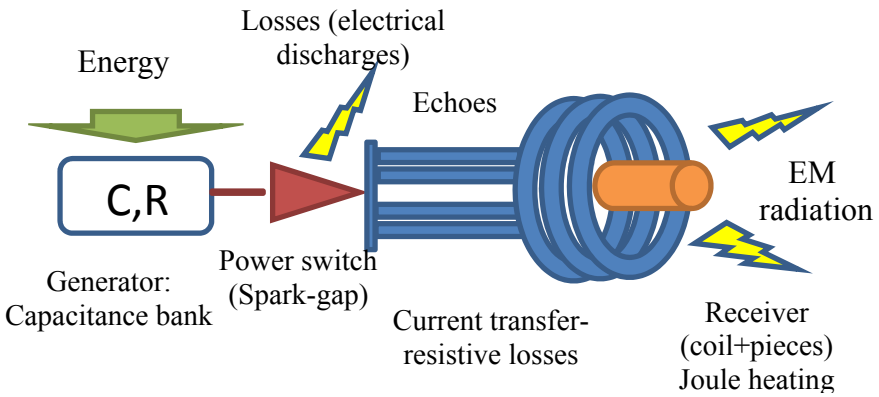

***Figure 1**: Typical structure of magnetic pulse machines indicating its main components and localization of the main EM radiation sources.*

This figure gives a simplified chart of the sources of energy loss. Electrical echoes in the current transfer lines result in both a distortion of the current pulses and substantial

resistive losses. EM radiation is produced especially by the spark-gaps (e.g. through electrical discharge) and the receiver (coil) fed by the very intense and short current pulses. A better understanding of such processes would help mastering the influence of the 'electromagnetic noise' on the machine dynamics and its optimization of the mechanism of the plastic deformation of pieces. The development of the underlying theory and its experimental validation is an essential step to understand the way the machine configuration and its structure influences the deformation process as well as a possible optimization of the welding or forming process through adaptation of the operating conditions to the mechanical properties of the tubes. In the search for relevant answers to these questions, we unavoidably have to face the structural complexity of these machines, manifesting in the coupling between its parts. To avoid the usual difficulties associated with the study of complexity, we carried out a global characterization of the machine and tried in a second step to capture its main structural and functional features through global electrical analogues, that is analogues of the whole machine. The necessary incorporation of the deforming tubes to the 'naked' machine analogue is not an easy task. Corrective attempts to the global analogues of the machine are proposed and discussed according to their interest in the understanding of the machine dynamics.

2 Electrodynamical Characterization: Results

A MP machine obviously underlies a more or less complex electrical circuit controlling its electrodynamic behavior. Aiming to build up a predictive and reliable framework accounting for the electrodynamics of MP machines, we thus need a global characterization of the electrical operating of these machines. Apart from a better understanding of their electrical features in view of their optimization, that framework allows also a monitoring to prevent their malfunction and over all, to assess their electrical structure. The electrical structure can be defined as the minimal set of parameters necessary to build the simplest global analogue of the machine, that is, the simplest electrical circuit accounting faithfully for its operating. The analogue provides the right interpretation of electrical measurements carried out on the machines. These parameters are of course intimately connected to the components of the machine and can be constrained by efficiency requirements.

To approach these questions and assess these parameters, we carried out such a complete characterization of the MP 25 9 magnetic pulse system developed by Pulsar (Ould Ahmed, 2012). In a first step, we have studied the 'unloaded' machine, that is, without insertion of the pieces to be deformed within the coil. The simplest global analogue of a MP machine as schematized in figure 1, consists in a classical RLC circuit corresponding to 3 parameters accounting for energy dissipation (combining the resistance of the transfer lines and the coil), the electrical energy stored in the power stage (bank capacitance) and the magnetic energy delivered by the coil (coil inductance). Other features as the coil geometry (dimensions, flat or massive) as well as special configurations of the machine's components are incorporated in these parameters. Uncontrolled coupling between the components might be responsible for deviations from the ideal operation of the machine (as defined in its

performance specifications). The typical current pulse (in kA) delivered by the machine is presented in **Fig. 2** below.

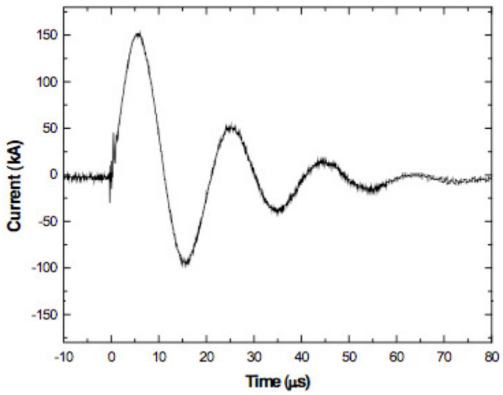

***Figure 2**: Profile of the current – pulse delivered by an MP machine (model MP 25 9 from the Pulsar Company). The pulse duration is typically 80 µs.*

Its profile evokes clearly a damped oscillator, which is the signature of a RLC circuit. The shots have thus been treated with a current profile,

$$I(t) = I_0 e^{-t/2\tau} \sin(\Omega t - \varphi) \qquad (1)$$

characterized by its maximal value I_0, the pulse duration τ (typically a few tenth microseconds), Ω the angular frequency and a phase angle φ accounting for the date of the rise of the current pulse.

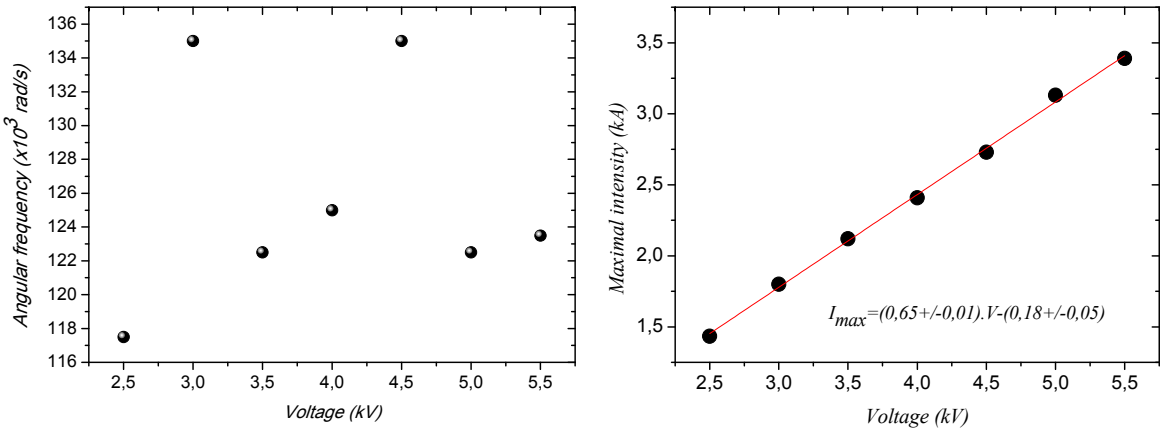

***Figure 3**: Dependence of the angular frequency (rad/s) – left panel - and maximal intensity (kA) – right panel - upon the feeding voltage V (kV) of the power stage.*

The dependence of the maximal intensity and the angular frequency upon the applied voltage across the power stage is presented on **Fig. 3** above. The evolution of the pulse duration and phase-angle is recapped on the left and right panels of **Fig. 4** below.

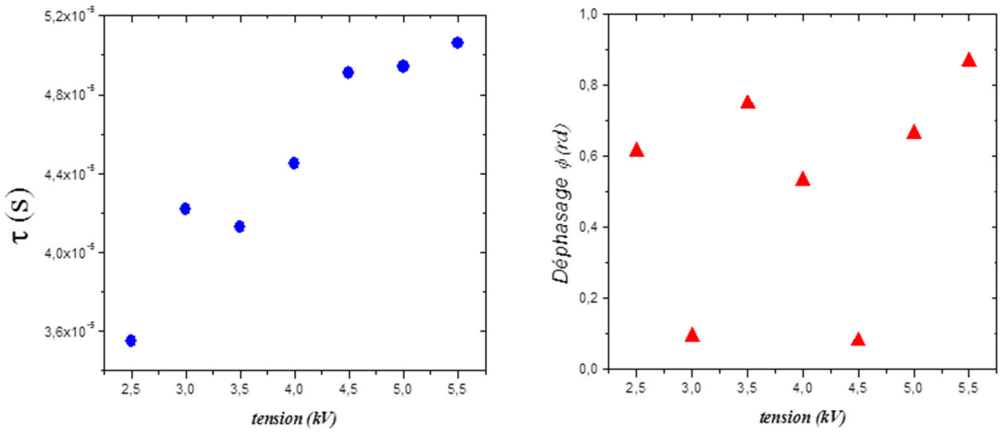

***Figure 4**: Dependence of the pulse duration (in s) – left panel – and the phase-angle (rad) – right pane – upon the feeding voltage (in kV) of the power stage.*

The angular frequency, the maximal current and the pulse duration are rather well defined with typical values of about 1,25 10^5 rad/s (or equivalently a frequency of 20 kHz) for the angular frequency and typical pulse duration varying slightly around 80 μs when the voltage doesn't exceed 6 kV. The pulse duration is defined as the time required for the measured intensity to vanish. The control of the current shape of the pulse through the feeding voltage is quite well ensured. This can be better appreciated on figure 3-b where the linear dependence is very well defined. The residue at zero-voltage has no physical meaning: it just indicates a systematic shift of the voltage measured across the power stage. Only the phase angle exhibits spread values, evidencing its random nature. This randomness manifests the difficulty with controlling the shot initiation, that is, their unsynchronized nature. The interpretation of these data is facilitated by the current pulse shape. As suggested by **Eq. 1**, the electrical structure of the MP system derives straightforwardly from a simple RLC circuit. Its parameters can then be assessed from the presented data. Considering the simplest case of as single shot initiated at a time t_0, the electrical behavior of the machine is modeled by the equation,

$$\frac{1}{C}\int I(t)dt + RI(t) + L\frac{dI(t)}{dt} = V(1-\theta(t-t_0)) \qquad (2)$$

where V is the constant feeding voltage of the power stage, I is the corresponding electric current and R, L and C are respectively the resistance, inductance and capacitance of the circuit. To avoid needless mathematical difficulties associated with the spark-gap operation, we have assumed here a rough discharge of the bank capacitance through a Heaviside

function $\theta(t-t_0)$ jumping at time t_0. Solving this equation requires an additional derivative leading to the Green equation,

$$\frac{1}{C}I(t)+R\frac{dI(t)}{dt}+L\frac{d^2I(t)}{dt^2}=-V\delta(t-t_0) \tag{3}$$

A simple Fourier transform followed by an integration in the complex plane leads to the current pulse ($t > t_0$),

$$\begin{cases} I(t)=\dfrac{4\pi V}{L\Omega}e^{-(t-t_0)/2\tau}\sin(\Omega(t-t_0)) \\ \Omega=\sqrt{\omega_0^2-1/4\tau^2}\ ,\tau=\mathrm{L/R},\omega_0=1/\sqrt{\mathrm{LC}} \end{cases} \tag{4}$$

This solution clearly accounts for the pulse shape given in Eq. 1 with a phase-angle $\varphi = \Omega t_0$. **Fig. 5** shows a plot of the measured current with its corresponding fit to a damped sine.

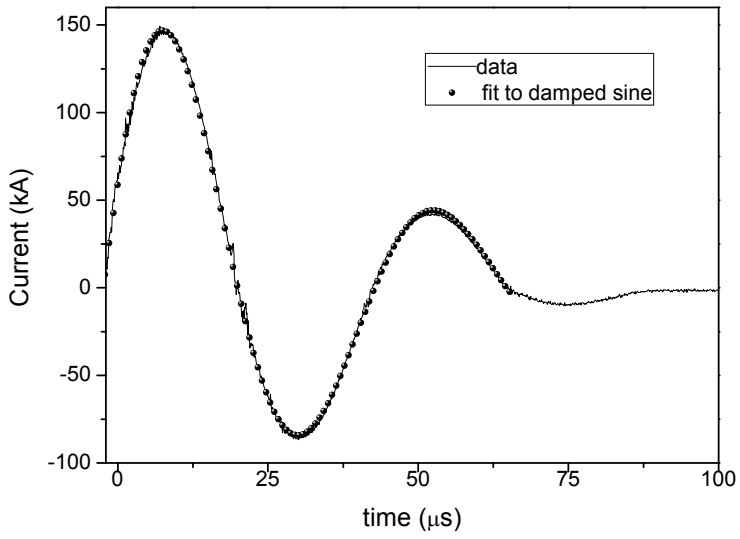

***Figure 5**: Plot of the experimental data (current (kA) vs. time (μs)) and its fit to a damped sine.*

The plot shows a good fit quality. We noticed that all our data can be fitted with a damped sine as our model suggests, but the quality of the fit is reduced at the last part before the end of the pulse, reflecting the high level of operation complexity of the spark-gaps power switches. This demonstrates that a more complete characterization of the machine is needed.

Comparison to the experimental data gives the following variations of the parameters in the applied voltage range,

$$\Omega/2\pi \simeq 20\ kHz,\ R \simeq 42-58\ \Omega,\ C \simeq 3{,}34.10^{-8}\ F,\ L \simeq 1{,}87\ mH$$

Taking into account the dispersion on the phase-angle values, the shot initiation dates vary within the time interval $t_0 \approx 4-6\ \mu s$. The assessment of the global resistance and the coil inductance are rather reasonable but the capacitance is questionable when compared to the expected (DC) capacitance of the power stage being a few hundredth microfarads. To solve this disagreement, we have to keep in mind that our model gives the effective parameters associated with the machine. The capacitance of the total circuit combines the power stage capacitance and additional contributions arising from the transfer line or any component of the machine. In our case, the additional contribution is attached to the coil slit (separation between two parts of the coil) which, being small, dominates the overall capacitance. Such perturbations regard in fact all the components of the machine, the critical ones being the capacitance and the coil inductance which determine the current (and magnetic) pulse duration and the working frequency ω_0. A too high shift of this working frequency can affect the quality of the welding or forming processes. Prior to any trial, an adequate preparation of the machine is thus necessary. This optimization of the configuration can only be reached through a careful characterization of the system.

3 Estimation of the Magnetic Fields: Theoretical and Numerical Modeling

The magnetic pulse is delivered by the coil excited by the current pulse studied in the previous section. In the present section, we enunciate a tentative assessment of the magnetic field created by the coil. This study follows logically the first step dedicated to the MP system electrodynamic characterization and consists in both the numerical computation of the current distribution (Foy, 2013) within the coil bulk and the magnetic field (intensity) distribution created by the coil. To achieve this goal despite the complexity of the situation, a simplified model was derived from reasonable assumptions. The first simplification regards the dimensionality of the numerical model restricted to 2D, allowing handling simpler boundary conditions. In a 2D space, the magnetic field reduces to a (pseudo-) scalar, being in fact the component of the field perpendicular to the coil plane.

The Maxwell-Ampère equation then reads,

$$J.\nabla B = \mu_0 \vec{j} + \frac{1}{c^2}\partial_t \vec{E}, J = \begin{pmatrix} 0 & 1 \\ -1 & 0 \end{pmatrix} \quad (5)$$

The left-hand side of this equation corresponds to the usual curl term and *J* the right angle is the rotation matrix in the plane. *B* and *E* represent the magnetic field and the electric field, respectively. From this equation we deduce the field gradient, expressed as a function of the displacement current (derivative of the electric field) and the conduction current (Ohm's law)

$$\nabla B = -\mu_0 J.\left(\int_{-\infty}^{+\infty} \sigma(t-t')\,\vec{E}(t')dt' + \varepsilon_0 \partial_t \vec{E}\right) \quad (6)$$

A time-Fourier transform of this expression leads to the (Fourier amplitude) electric field,

$$\begin{cases} \vec{E}_\omega = \frac{1}{\mu_0(\sigma(\omega)+\varepsilon_0 i\omega)} J.\nabla B_\omega = i\omega J.\nabla\varphi_\omega \\ \varphi_\omega = \frac{B_\omega}{\mu_0(i\omega\sigma(\omega)-\varepsilon_0\omega^2)} \end{cases} \quad (7)$$

In the expression of the potential φ_ω , $\sigma(\omega)$ is the complex conductivity of the coil material, that is, the FT of the response function σ(t) in **Eq. 6**. Within the approximation of quasi-steady regime ($\omega \ll \sigma/\varepsilon_0$) in which propagation effects are negligible, we are led to simpler equations,

$$\begin{cases} \varphi_\omega \simeq \frac{B_\omega}{\mu_0 i\omega\sigma(\omega)} \\ E_{\omega x} = \partial_y(B_\omega/\mu_0\sigma(\omega)) \\ E_{\omega y} = -\partial_x(B_\omega/\mu_0\sigma(\omega)) \end{cases} \quad (8)$$

These equations state that the current stream lines are perpendicular to the isolines of the potential φ. The main difficulty of the model relies on skin effect. Understanding its influence on the fields and the current distribution doesn't require solving these equations in the whole frequency range. For practical use, the low (LF) and high (HF) frequency limits of **Eq. 7**, detailed in **Eq. 9**, provide the relevant information.

$$\begin{cases} \vec{E}_\omega \simeq J.\nabla\varphi_\omega^{LF} \\ \varphi_\omega^{LF} \approx \frac{B_\omega}{\mu_0\sigma_{DC}}, \sigma_{DC} = \sigma(0) \end{cases} \quad \begin{cases} \vec{E}_\omega \simeq J.\nabla\varphi_\omega^{HF} \\ \varphi_\omega^{HF} \approx \frac{B_\omega}{\mu_0\sigma(\omega)} \end{cases} \quad (9)$$

The threshold separating these two regimes is given by the characteristic frequency σ/ε_0, which is about 1,6 MHz for Fe and about 300 kHz for stainless steel. Handling these limits separately allows avoiding difficulties with the treatment of the rigorous equations. In most MP systems, the operating frequencies being a few tenth kHz are low enough (compared to σ/ε_0) to justify the restriction to the LF limit. The LF limit equations were thus solved through a finite element (FE) method implemented within the Matlab software (using PDE Toolbox). The mesh was composed of 8496 triangles, 4405 nodes and 316 edges. We used a full integration method. The LF solution obtained for an excitation current $I = 10^5$ A, which is a realistic value for our shots, is presented on **Fig. 6** below.

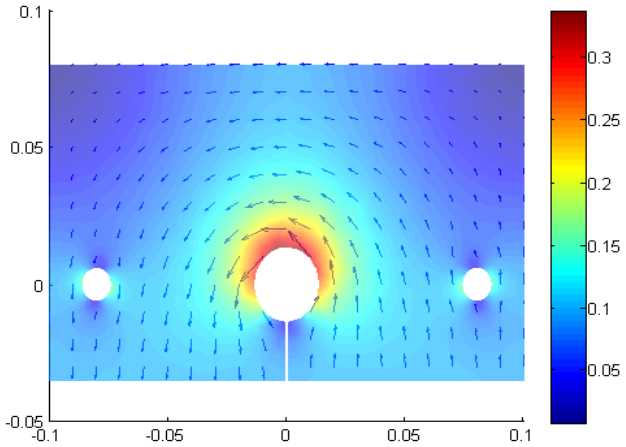

***Figure 6**: Distribution of the current stream lines with the coil material and corresponding variation of the electric field intensity.*

This figure gives the space variation of the electric field amplitude within the coil bulk as well as the current streamlines. Using the Biot-Savart law, we derived from this current distribution the magnetic field amplitudes generated by the coil for different types of metallic materials. To match the 3D realistic situation, we inserted the coil thickness *h* along the axis (in our case $h = 1.5$ cm) in a frequency-scaling law obeyed by the Fourier amplitude of the magnetic field,

$$\vec{B}(\omega) = \frac{\mu_0}{4\pi}\sigma_{DC} h \sqrt{\omega}\,\vec{B}(1\ rad/s) \qquad (10)$$

This relation allows to deduce the solution at any (low enough) frequency from the simulation at a fixed frequency of 1 rad/s. The variation ranges of the magnetic field generated by the coil are reported in **Table 1** along with the corresponding magnetic pressure evaluated at the operating frequency of the machine, that is 20 kHz.

Material	Variation range (Teslas)	Magnetic pressure (kPa)
Stainless steel	**0,097 - 0,16**	**3,7 - 10**
Iron	**0,97 - 1,62**	**37 - 100**
Copper	**5,8 - 9,72**	**13330 - 37600**

***Table 1:** Variation range of the magnetic field intensity (Teslas) for different metallic materials and corresponding magnetic pressure (kPa).*

Obviously, the great difference between these values reflects the importance of the choice of the metallic compound (its conductivity). These values seem reasonable. While all of these materials (especially stainless steel and iron) would of course not be relevant for these applications, this table only shows estimates for such materials in order to compare

them. Nevertheless, our ideal model assumes a 'perfect' coil, that is, without defects. An extension of the model to more realistic coils with bulk defects might be interesting to evaluate field inhomogeneities, since these alterations of the magnetic field can deeply affect the welding/forming process and its quality.

4 Welding Configuration: Insertion of Metallic Tubes

This section is devoted to a preliminary study of the local electrical analogue associated with the deformable pieces coupled to the coil generator. In welding configuration, the metallic coaxial tubes to be deformed are inserted in the coil. This additional component modifies the structure of the global electrical analogue of the machine. The additional circuit associated with the {coil + pieces} subsystem plays in fact the role of the receiver (of the energy delivered by the MP system) and can have a complex structure. The main difficulty with the identification of that structure arises mainly from the electromagnetic coupling between the coil and the metallic pieces. The simplest approach to the problem consists in a parallel self/capacitor device. The capacitor reflects the geometrical configuration of the coaxial tubes: this is a cylindrical capacitor with a capacitance given by the usual formula $C = 2\pi\varepsilon_0 l / Ln(R_2 / R_1)$, for tubes of length l and radii R_2 for the external tube, R_1 for the internal tube. The inductance component accounts for the eddy current excited within the tubes and the magnetic energy stored within. A resistance modeling the dissipative effects can be added. This minimal electrical analogue accounts for the mutual inductance coupling between the coil generator and the tubes (transformer configuration) and controlling the energy transfer to the tubes. It is clear that the knowledge of this magnetic coupling is of great importance, especially with respect to efficiency questions. Indeed, the impedance introduced by this additional circuit varies very rapidly because of the fast deformation kinetics of the tubes: we have to deal with strongly time dependent components, making it difficult to ensure impedance matching between the power stage and the coil generator stage. This type of unsteady circuit, whose structure varies rapidly with time, is very difficult to handle because of a lack of both theoretical and experimental knowledge. From an experimental point of view, a deeper electrical characterization is clearly needed. Up to now, our theoretical and experimental investigations pointed out some research directions. Retaining the only capacitance of the tubes, we built up a simplified model of the local electrical analogue incorporating the coupling between the electrical degrees of freedom (charge $Q(t)$) and the mechanical ones (deformation $x(t)$). This model is depicted in **Fig. 7** where the spring models the elastic properties of the tubes and $e(t)$ is the voltage between the tubes (plates of the capacitor). This voltage is a residue of the inductance of the tube (not explicit in this model), that is, the voltage induced by the varying magnetic flux through the tube.

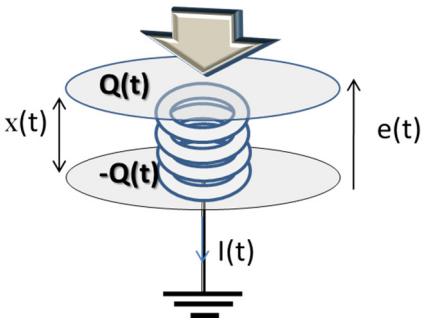

***Figure** 7: Schematic view of the simplest electrical analogue of two coaxial elastic tubes evidencing the coupling between the mechanical and electrical degrees of freedom.*

Ignoring in a first step the dissipation, the dynamics of such a system derives from the Lagrangian,

$$L(x,\dot{x}) = \frac{1}{2}M\dot{x}^2 - \frac{1}{2}k(x(t)-\bar{x})^2 + F_m(t)x(t) - \frac{1}{2}C(x(t))e(t)^2 \qquad (11)$$

The first terms give the mechanical contribution including the magnetic force F_m, the last one, giving the electrical energy stored in the deformable pieces, generates the coupling between the mechanical and electrical degrees of freedom. It admits series expansion in powers of the deformation $\Delta(t) = x(t) - \bar{x}$, leading to the dynamical equation corrected by a dissipative force,

$$\begin{cases} \ddot{\Delta} + \omega_0^2(t)\Delta + \eta\dot{\Delta} = F_m(t) - \frac{1}{2}\frac{\partial C}{\partial x}(\bar{x})e(t)^2 \\ \omega_0^2(t) = \frac{k}{M} + \frac{1}{M}\frac{\partial^2 C}{\partial x^2}(\bar{x})e(t)^2 \end{cases} \qquad (12)$$

This equation has a complex structure, as could be expected. It evidences the influence of the voltage *e(t)* on both the 'resonance' frequency of the tube and the magnetic pressure force. The consequence of these effects on the dynamics of the tube is made simpler for a constant voltage: the resonance frequency is simply shifted. At high enough voltage, the matching between the mechanical resonance frequency of the tube and the operating frequency of the machine (required for high quality welding) is lost. On the other hand, it strengthens the magnetic force exerted on the tube (since the derivative is negative). As the induced voltage depends in a complex way upon the current pulse and its derivative, the Fourier spectrum of the deformation is strongly altered. A deeper understanding of these effects requires additional experimental studies and can profit by the measurement of the deformation kinetics law (Deroy, 2015). A fundamental application of this preliminary investigation devoted to the identification of electrical analogues of the pieces inserted in the coil generator, concerns a new type of spectroscopy of the tubes. Our proposal exploits the natural configuration of the pieces and the coil in the welding machine. We expect two different configurations of the device:

- Deformation spectroscopy mode: the tubes are excited by a ‘low amplitude’ modulated magnetic field. This mode allows in situ mechanical testing of the tubes prior to any welding process.

- Deformation kinetics of the tubes in the welding regime. This application should lead to a more complete understanding of the plastic deformation kinetics of the tubes.

The implementation of these techniques will certainly lead to relevant global electrical analogues of any MP system, especially in view to optimize the welding or forming process.

5 Conclusion

We carried out a theoretical, experimental and numerical study of MPW machines.

The classical setups of such machines are depicted, and because of their inherent complexity, electrical analogues are used in order to ease their physical description.

A first magnetic pulse system is treated as a RLC circuit, with its components being experimentally and separately characterized. The main parameters of such a circuit can then be deduced. While the coil inductance and global resistance can be considered reasonable, a problem lies with the capacitance. This is due to the fact that only the bank (power stage) capacitance was taken into account in our early model, while other contributions, such as the capacitance arising from the coil slit, were not included.

A further study, using numerical tools, allowed for the computations of current distributions within the coil bulk, along with the magnetic field such currents create within the coil. Using the electromagnetism equations (namely, the Maxwell-Ampère equation) for a 2D model, we calculate the corresponding Fourier transforms of such solutions so that two limits appear: low and high frequencies. We show that low frequencies are of interest for us on MP machines and solve the LF equations using a PDE toolbox in Matlab. We then get the values of the current distributions within the coils and corresponding magnetic fields, and the magnetic pressure values they generate.

The last part of our paper deals is of theoretical nature, and deals with the true configuration of the machine, that is when metallic tubes are inserted. Using the Lagrangian formalism, the dynamics of the tubes are modeled, taking into account their capacitive properties. While this part is only theoretical, it may lead to two interesting measurement processes: a deformation spectroscopy mode, allowing in situ mechanical testing of the tubes without any welding, and another mode, which should allow for a greater understanding of the process of plastic deformation of the tubes.

Acknowledgments

We wish to thank the Région Picardie for its support.

References

Broeckhove J., 2010. Experimental research on magnetic pulse welding of dissimilar metals. Ph.D. Thesis, Ghent University, Belgium.

Daehn G. S., 2002. High Velocity Sheet Metal Forming: State of the Art and Prognosis for Advanced Commercialization, Ohio State University Press.

Deroy J., Avrillaud G, Ferreira S., Jeanson A.C., 2015. Comparison between experimental and simulated velocities in MPW geometry. In: I2FG Dortmund 2015, Dortmund, Germany.

Foy N, 2013. Soudage par impulsions magnétiques. Physics M.S. internship report, Université de Picardie Jules Verne, Amiens, France.

Griffith D.J., 1999. Introduction to electrodynamics. Prentice Hall, New Jersey.

Ould Ahmed S.M., 2012. Electrodynamique des machines de soudure à impulsions magnétiques. Physics M.S. internship report, Université de Picardie Jules Verne, Amiens, France.

Psyk, V., Risch, D., Kinsey, B.L., Tekkaya, A.E., Kleiner, M., 2011. *Electromagnetic forming – A review*. Journal of Materials Processing Technology 211 (5), pp. 787-829.